Available online at www.sciencedirect.com
ScienceDirect
Ceramics International 38 (2012) 627–634
CERAMICS INTERNATIONAL
www.elsevier.com/locate/ceramint

Low temperature synthesis of monolithic mesoporous magnetite nanoparticles

Rkia El-kharrag [a], Amr Amin [a,**], Yaser E. Greish [b,*]

[a] Department of Biology, College of Science, United Arab Emirates University, Al Ain, P.O. Box 17551, United Arab Emirates
[b] Department of Chemistry, College of Science, United Arab Emirates University, Al Ain, P.O. Box 17551, United Arab Emirates

Received 22 June 2011; received in revised form 22 July 2011; accepted 23 July 2011
Available online 30th July 2011

Abstract

Magnetite nanoparticles are commonly used for drug delivery, as MRI contrast agents, and as adsorbents for the removal of heavy metal cations from waste water. The smaller the particle sizes the higher the efficiency of these particles in these applications. Different methods have been explored for the preparation of magnetic nanoparticles with this size limitation. Co-precipitation is one of the most versatile methods in this regard, and is characterized by the ability of preparation of a high yield of nanoparticles. Control of the particle size distribution, phase purity and type of porosity of the formed magnetite nanoparticles has been always considered a challenge. In the current study, magnetite mesoporous nanoparticles with an average particle size of 55 nm were prepared in pre-adjusted highly alkaline aqueous media at relatively low temperatures. Phase purity of the deposited magnetite was confirmed by X-ray diffraction (XRD) and thermogravimetric analysis (TGA). Scanning (SEM) and transmission electron microscopy (TEM) graphs showed homogenously dispersion of spherical magnetite nanoparticles. Agglomeration of the mesoporous nanoparticles took place forming clusters with unified pore size distribution due to the homogenous particle size distribution. Magnetic susceptibility measurements at room temperature confirmed the magnetization characteristics of the nanoparticles.

Keywords: Magnetite nanoparticles; Co-precipitation; Mesoporous; Phase composition; Microstructure; Magnetic susceptibility

1. Introduction

Interest in magnetite nanoparticles has dramatically increased in the past two decades for its wide scope of applications [1–10]. Biomedical applications, such as targeted drug delivery [3], require that the magnetite nanoparticles have high magnetization values, a size smaller than 100 nm, a narrow particle size distribution, and a biocompatible surface coating that allows for a targetable delivery with particle localization in a specific area. In addition, magnetite nanoparticles have been used as adsorbents for the removal of heavy metal cations from waste water, which also requires low and homogeneous particle size distribution to achieve an enhanced efficiency [11]. Moreover, having mesoporosity in the magnetite nanoparticles widens its scope of applications in catalysis, separation, and drug delivery [12,13]. Magnetite nanoparticles, especially those coated with biocompatible polymers, can bind to drugs, proteins, enzymes, antibodies, or nucleotides and can be directed to an organ, tissue, or tumor using an external magnetic field [14]. Polymers containing certain chelating groups, such as –COOH and $–NH_2$, have been also used to increase the affinity of mesoporous magnetite nanoparticles towards heavy metal pollutants in waste water [11]. For example, magnetite nanoparticles were shown to bind As (III) and As (IV) ions, which are common heavy metal pollutants, from waste water with high efficiency [15,16].

Various methods have been investigated for the preparation of magnetite nanoparticles [17–23]. Among those, co-precipitation is the simplest and most efficient method, especially if high yield of the magnetite nanoparticles is the main objective [24–26]. In this method, magnetite is prepared by one of two procedures: controlled oxidation of Fe^{2+} aqueous solutions in an alkaline media to produce Fe^{2+} and Fe^{3+} with a molar ratio of 1:2, respectively (same as that in magnetite) [27], or by an addition of a high pH alkaline solution to an aqueous mixture of Fe^{2+} and Fe^{3+} originally mixed at a molar ratio of

* Corresponding author. Permanent address: Department of Ceramics, National Research Centre, Cairo, Egypt. Tel.: +971 50 2338203.
** Corresponding author. Tel.: +971 50 7437039.
E-mail addresses: a.amin@uaeu.ac.ae (A. Amin), y.afifi@uaeu.ac.ae (Y.E. Greish).

0272-8842/$36.00
doi:10.1016/j.ceramint.2011.07.052

1:2, respectively [28–31]. In the first procedure, controlled oxidation of Fe^{2+} might not be valid, and as a result a mixture of iron oxides, rather than magnetite, is produced. In the later method, reaction takes place as shown in Eq. (1) [32–34]:

$$Fe^{2+} + 2Fe^{3+} + 8OH^- \rightarrow Fe_3O_4 + 4H_2O \quad (1)$$

According to the thermodynamics of this reaction, a complete precipitation of Fe_3O_4 should be expected between pH 9 and 14, while maintaining a molar ratio of Fe^{3+}:Fe^{2+} as 2:1 under a non-oxidizing oxygen-free environment [32]. Otherwise, Fe_3O_4 might also be oxidized as given in Eq. (2):

$$Fe_3O_4 + {}^1/_4\,\mathbf{O}_2 + 4{}^1/_2\,\mathbf{H}_2O \rightarrow 3Fe(OH)_3 \quad (2)$$

Co-precipitation in oxygen-free environment is carried out by bubbling N_2 gas through the solution [32]. This was found to protect critical oxidation of the magnetite and reduce the particle size when compared with methods without removing the oxygen [24,35]. Another crucial parameter that has to be monitored throughout the wet synthesis of magnetite nanoparticles is the pH of the medium, both during the synthesis process as well as during the purification/washing of the formed nanoparticles. The current study investigates the synthesis of mesoporous magnetite nanoparticles via a co-precipitation in a pre-prepared highly alkaline medium in air at low temperatures. The current modified co-precipitation process ensures the formation of monolithic magnetite nanoparticles where thermodynamics of the process was adjusted so that formation of lower oxides and hydroxides are avoided. Optimization of the process was carried out through studying the effects of feeding rate of the starting Fe^{2+}/Fe^{3+} mixture into the basic medium, the stirring and soaking temperatures, as well as the ionic strengths of the medium. Characterization of the formed magnetite nanoparticles was carried out by XRD, TGA, SEM, TEM and magnetic susceptibility measurements at room temperature.

2. Materials and methods

Chemicals used in the current study included iron (II) chloride tetrahydrate ($FeCl_2{\cdot}4H_2O$), iron (III) chloride ($FeCl_3$), sodium hydroxide (NaOH) and ammonia solution. All reagents were analytical-grade and were purchased from Sigma–Aldrich, USA. Aqueous solutions of Fe^{2+} and Fe^{3+} were separately prepared by dissolving the respective amounts of $FeCl_2{\cdot}4H_2O$ and $FeCl_3$ in de-ionized water. To study the effect of varying the ionic strengths of the starting solutions on the characteristics of the formed nanoparticles, Fe^{2+}/Fe^{3+} solutions containing 0.075/0.15, 0.15/0.3, 0.3/0.6 or 0.6/1.2 were investigated. An aqueous solution of NaOH of pH 13 was also prepared by dissolving the corresponding amount of NaOH in de-ionized water. A pre-calculated volume of the NaOH solution was heated to a pre-decided temperature in an open round flask. A mixture containing equal volumes of Fe^{2+} and Fe^{3+} was injected into the NaOH solution at feeding rates of 20, 40 or 60 mL/h, with vigorous stirring. At the end of addition, a brownish-black precipitate was formed. The whole solution was vigorously stirred at the same constant temperature. The effect of varying the stirring temperature on the physical characteristics of the formed nanoparticles was studied by keeping stirring temperatures at 60, 70, 80 or 90 °C. Magnetite suspensions were then soaked at 60, 75 or 90 °C for 24 h. The magnetite suspensions were then centrifuged at 3000 rpm for 15 min followed by a successive decantation/washing with 12% ammonia solution for 3 times. After a final decantation, magnetite deposits were collected and dried at 60 °C for 24 h. Dried powders were finely ground to be characterized for its composition, morphology, surface area, and magnetic susceptibility.

Composition of the prepared magnetite was studied by XRD. An automated X-ray diffractometer, with a step size of 0.02°, scan rate of 2°/min, and a range from 2θ = 10–70° was used. Solid magnetite samples were evaluated for their microstructures using a JEOL SEM at an accelerating voltage of 15 kV. Average particle size of the prepared nanoparticles was assessed from the samples micrographs by careful analysis of a selected area of the same dimensions in the samples micrographs. Detailed description of the morphology of the nanoparticles was examined by TEM; CM10 – Philips Transmission Electron Microscope, Netherlands, Holland. TGA was also used to investigate the thermal properties of the prepared nanoparticles using a TGA-50 Shimadzu. Thermogravimetric Analyzer where pre-weighed powder samples were heated to 600 °C at a heating rate of 20 °C/min. BET surface area, porosity, pore size distribution and pore volume of the dried solid samples were measured using nitrogen gas adsorption at 77 K employing a Quantochrome NOVA 1000 volumetric gas sorption instrument; Autosorb, USA. Pore size distribution was calculated using the DLJ method for the desorption segment of the hysteresis curve of each sample. Magnetic susceptibility measurements were carried out at room temperature using a magnetic susceptibility balance (MSB-Auto, Sherwood Scientific Ltd., England). A pre-determined mass of finely ground magnetite nanoparticles was filled in a narrow glass tube and was subjected to a constant magnetic field of 4.5 kGauss. Data were expressed as mass susceptibility (χ_g) in m^3/kg, which is directly related to the magnetization.

3. Results and discussion

Formation of different types of iron oxides in aqueous media has been studied from the electrochemical point of view using Pourbaix diagrams [36]. A schematic Pourbaix diagram showing the areas of thermodynamic stability of various iron oxide and hydroxide phases is shown in Fig. 1. Magnetite precipitates as a stable phase in highly basic aqueous media where the precipitated magnetite nanoparticles acquire negative charges on their surfaces [36]. Illés and Tombácz [37] showed an isoelectric point (IEP) of 8 above which particles developed a negative charge. Negativity of the magnetite surfaces increase with increasing the alkalinity of the medium. Moreover, zeta-potential measurements of pure magnetite sols showed a point of zero charge (PZC) of 8.2,

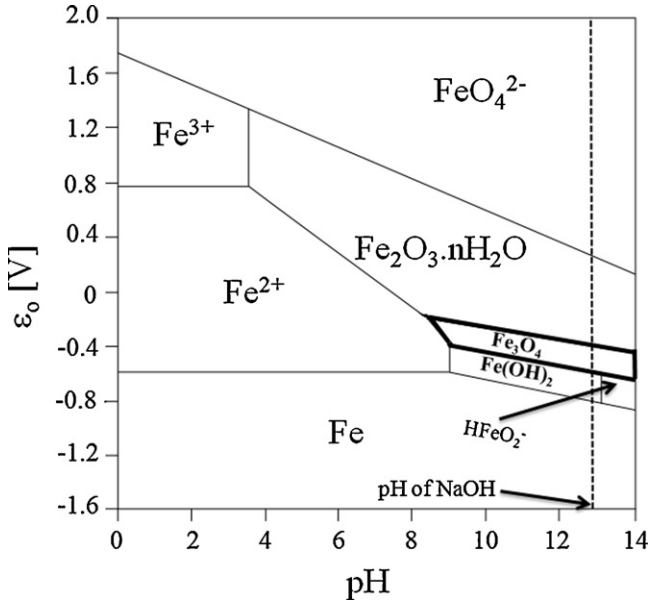

Fig. 1. Pourbaix diagram for the iron–water system showing the thermodynamically stable phases in aqueous solutions with various pH values [36].

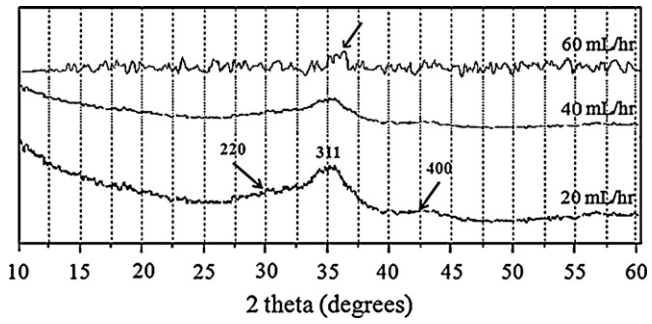

Fig. 2. X-ray diffraction patterns of solid magnetite samples prepared at different feeding rates of the Fe^{2+} and Fe^{3+} aqueous solutions.

which is in a close agreement with the IEP value [38]. These facts were previously used for electrostatic stabilization of the nanoparticles in their solutions, where repulsion between the negatively charged nanoparticles prevented their agglomeration [39,40]. In highly basic aqueous media, Pourbaix diagrams indicated that other phases such as FeO_4^{2-}, Fe_2O_3, $Fe(OH)_2$ and $HFeO_2^-$ may also exist under these conditions. These phases could be distinguished from each other using various characterization techniques such as XRD and Infrared Spectroscopy (IR). In addition, magnetite, Fe_3O_4, has been viewed as an assembly of FeO and Fe_2O_3 [34]. When synthesized in air, FeO gets oxidized to Fe_2O_3, leaving a phase-pure Fe_2O_3, according to Eq. (3).

$$2(FeO \cdot Fe_2O_3) + {}^1/_2\,O_2 \rightarrow 3Fe_2O_3 \quad (3)$$

Oxidation reactions shown in Eqs. (2) and (3) explain why synthesis of magnetite in alkaline media in air has been always abandoned to avoid the formation of phase-impure Fe_3O_4. In the current study, phase-pure magnetite was prepared under alkaline conditions in air, as will be shown in the phase composition analysis of the formed nanoparticles. Fig. 2 shows the phase evolution during the formation of magnetite as a function of the feeding rate. It should be mentioned that both stirring and soaking temperatures as well as the starting concentrations of Fe^{2+} and Fe^{3+} were kept constant. The XRD patterns in Fig. 2 compare the crystallinity of magnetite formed at feeding rates 20, 40 or 60 mL/h. At a fast feeding rate of 60 mL/h, the deposited magnetite nuclei rapidly formed and accumulated without further crystallization leading to an amorphous phase, as was shown in Fig. 2, which also shows a relatively weak intensity peak at 2θ value of 35.2° for the 3 1 1 plane. This indicated the need for a slower rate of addition of the iron reactants. At a slower feeding rate of 40 mL/h, relatively more time was given for the deposited nuclei to crystallize. This was even increased by decreasing the feeding rate to 20 mL/h, as indicated by the presence of the magnetite characteristic peaks at 2θ values of 29.9° (2 2 0), 35.2° (3 1 1), and 43.1° (4 0 0). In addition to these findings, no indication for the presence of non-magnetite phases was observed despite the

Table 1
Effect of different optimization conditions on the average particle size and surface area of magnetite nanoparticles prepared through a co-precipitation in an aqueous solution containing $FeCl_2$, and $FeCl_3$ as starting reagents.

$[Fe^{2+}]/Fe^{3+}]$	Feeding rate (mL/h)	Stirring temperature (°C)	Soaking temperature (°C)	Average particle size (nm)	Surface area (m^2/g)
0.30/0.60	20	60	60	76	197
0.30/0.60	40	60	60	55	215
0.30/0.60	60	60	60	85	167
0.30/0.60	40	60	60	55	215
0.30/0.60	40	70	60	165	140
0.30/0.60	40	80	60	290	81
0.30/0.60	40	90	60	350	72
0.30/0.60	40	60	60	55	215
0.30/0.60	40	60	75	165	140
0.30/0.60	40	60	90	189	122
0.015/0.30	40	60	60	55	215
0.15/0.30	40	60	60	120	188
0.30/0.60	40	60	60	165	175
0.60/1.20	40	60	60	175	162

fact that the entire preparation process took place in air. The effect of changing the feeding rate on the average particle size and surface area of the deposited magnetite nanoparticles is shown in Table 1. Despite the difference in crystallinity of the formed nanoparticles at different feeding rates, a less pronounced variation in the average particle size was detected.

Given the phase purity of magnetite formed at these conditions, a feeding rate of 40 mL/h was chosen for the optimization of the following preparation parameters. Stirring temperature during and after the addition of the Fe^{2+} and Fe^{3+} ions to the pre-adjusted alkaline solution was varied at 60, 70, 80 or 90 °C. This is shown in Table 1 to have a pronounced effect on the average particle size and surface area of the formed nanoparticles without affecting the overall crystallinity or purity of the magnetite nanoparticles. The least particle size of 55 nm was achieved at a stirring temperature of 60 °C. Size increased by raising the stirring temperature up to 90 °C. Previous researchers have shown that only kinetic factors are controlling the growth of the crystal [41]. In a co-precipitation process where Fe^{2+} and Fe^{3+} ions are added at the same time, the mechanism of precipitation of magnetite takes place over two stages [42–47]. The first stage involves a short burst of nucleation as the concentration of the species reached critical supersaturation. This step is followed by a slow growth of the nuclei by diffusion of the solutes to the surface of the formed magnetite crystallites. This step is believed to be enhanced by increasing the stirring temperature during the addition of the iron species. Moreover, and in contrast to an average size of 15 and 26.5 nm of the magnetite nanoparticles obtained at a stirring temperature of 80 °C under N_2 gas in the work of Zhang et al. [48] and Lee et al. [49], the relatively higher size obtained in the current study; at 60 °C, could be attributed to the fact that all preparations were carried out in air. At a lower temperature range (4–37 °C), and using $NaNO_2$ as an oxidant, a controlled oxidation of Fe^{2+} in an alkaline media under N_2 gas took place forming magnetite nanoparticles with a size range of 30–100 nm [27]. Although reactants used in this system are different from the currently studied one, its findings indicate that despite the presence of N_2 atmosphere, nanoparticles with a relatively large size could be obtained at temperatures below 60 °C.

After complete addition of reactants, precipitated magnetite nanoparticles were maintained in contact with their alkaline solutions for 24 h at soaking temperatures of 60, 75 or 90 °C. Soaking of the magnetite precipitates at relatively high temperatures following their co-precipitation was previously shown to enhance crystallinity, and was also shown to be a function of the soaking temperature [50]. The effect of varying the soaking temperature on the average particle size and surface area of the nanoparticles is given in Table 1. No change was observed in the size and surface area of the nanoparticles when the suspensions were soaked at the same temperature as that maintained during the addition and stirring of reactants. Increasing the soaking temperature up to 90 °C led to an increase in the particle size accompanied by a consequent decrease in the surface area of the formed nanoparticles. This indicates that the observed growth of the formed nanoparticles is temperature-dependent. It should be mentioned that varying

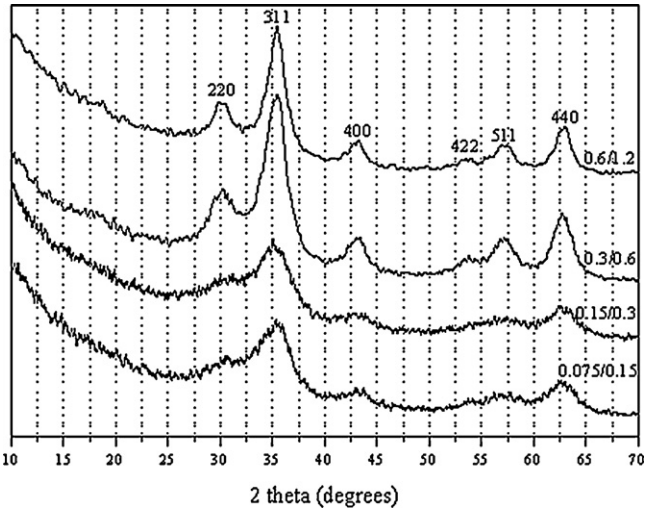

Fig. 3. X-ray diffraction patterns of solid magnetite samples prepared in solutions containing different initial concentrations of Fe^{2+} and Fe^{3+} ions.

the soaking temperature did not affect the crystallinity of the formed nanoparticles. It was, therefore, recommended to maintain the stirring and soaking temperatures at the same value. Based on these findings, magnetite nanoparticles prepared in solutions containing different concentrations of Fe^{2+} and Fe^{3+} were further characterized in more details. The data shown in Table 1 indicate that doubling the initial concentrations in the same constant volume of the alkaline solution resulted in a pronounced increase in the average size of the precipitated nanoparticles, with a consequent decrease in the surface area of the nanoparticles. This was also reflected in an increase in the crystallinity of the formed magnetite nanoparticles. Fig. 3 shows XRD patterns of magnetite powders deposited out of solutions containing various concentrations. Peaks appeared at 2θ values of 29.9° (2 2 0), 35.2° (3 1 1), 43.1° (4 0 0), 53.4° (4 2 2), 57.1° (5 1 1), and 62.8° (4 4 0) were observed in all samples, and are consistent with the standard data of phase-pure magnetite [49,51,52]. Despite the fact that

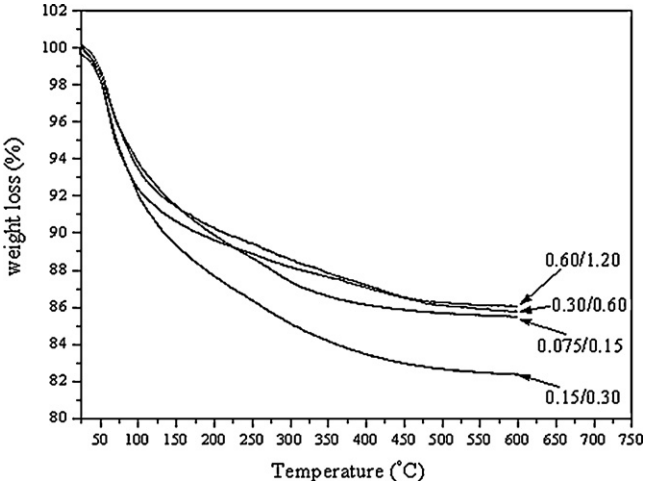

Fig. 4. Thermogravimetric analysis of solid magnetite samples prepared in solutions containing different initial concentrations of Fe^{2+} and Fe^{3+} ions.

the current experiments were carried out in air, no sign of oxidation of the formed magnetite was found, reflecting its chemical stability. The relative broadening of the peaks at 29.9°, 35.3° and 62.8° in samples made of solutions containing Fe^{2+}/Fe^{3+} 0.075/0.15 ratio is attributed to relatively small particle size, which is known to result from dilute solutions [49]. Nedkov et al. [53] observed the formation of vacancies on the surface of magnetite nanoparticles with size below 12.5 nm without a further oxidation to maghemite. The least particle size observed in the current study was 55 nm. The absence of maghemite in the XRD patterns of the magnetite nanoparticles prepared in the current study does not exclude the possibility of formation of vacancies on their surfaces, but confirms the phase purity of the prepared magnetite nanoparticles.

Fig. 4 shows TGA graph for magnetite samples, prepared from solutions containing various concentrations of the initial

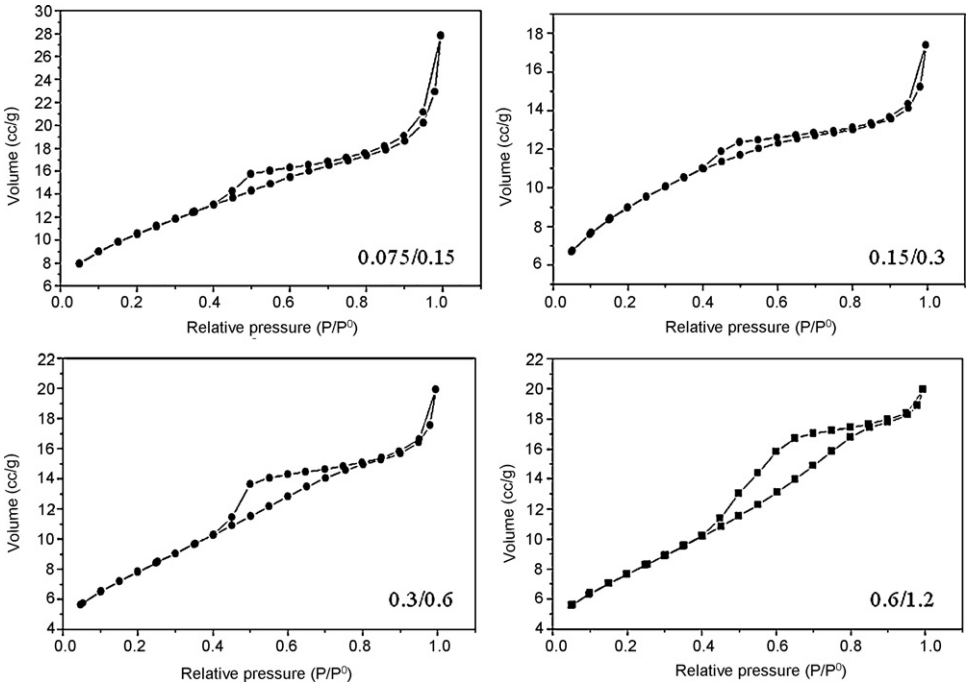

Fig. 5. Adsorption isotherms of solid magnetite samples prepared in solutions containing different initial concentrations of Fe^{2+} and Fe^{3+} ions.

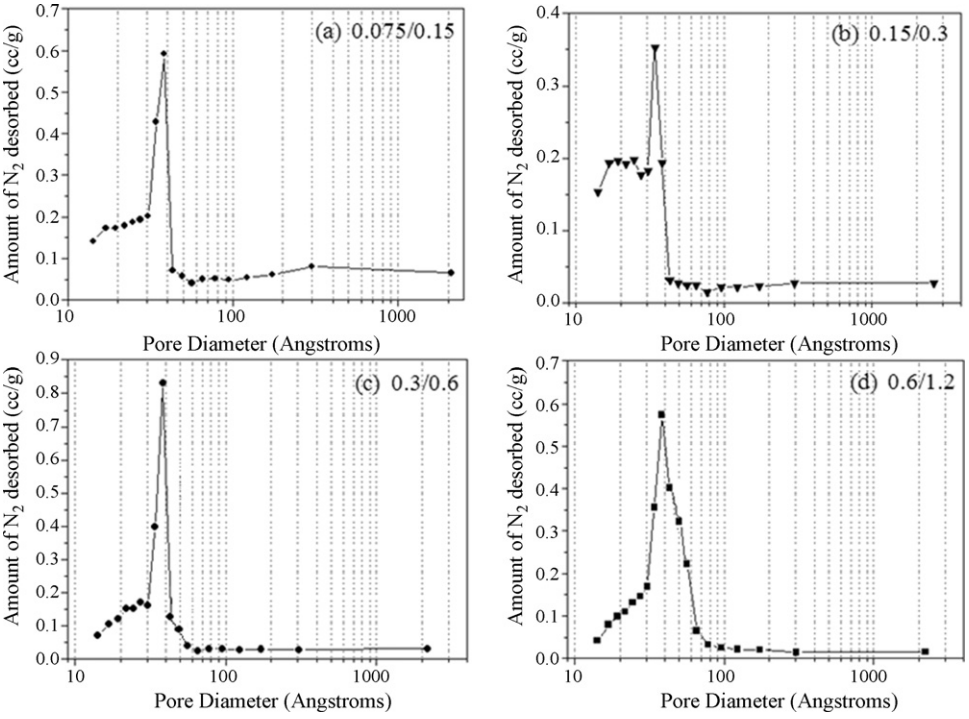

Fig. 6. Pore volume distribution in solid magnetite samples prepared in solutions containing different initial concentrations of Fe^{2+} and Fe^{3+} ions.

Fe^{2+}/Fe^{3+} solutions. All samples showed weight loss values in the range of 14–17% taking place at a mid temperature of 100 °C. This is attributed to the evaporation of the physically adsorbed water. This loss continued to take place with a slower rate as temperature increased. This could be attributed to the presence of multi layers of water of hydration on the surfaces of the nanoparticles. It should be mentioned that after complete dryness of all powders, nanoparticles were highly agglomerated, which is a common characteristic of small nanoparticles prepared in aqueous media. Fig. 5 shows the adsorption isotherms of N_2 on agglomerated powders prepared from solutions containing various concentrations of the initial Fe^{2+}/Fe^{3+} solutions. All samples showed hysteresis loops of type IV where the lower curve represents the adsorption of N_2 gas on the surfaces of the nanoparticles, while the upper curve represents the progressive withdrawal; desorption, of the adsorbed N_2 gas [54]. As a result of the isotherms in Fig. 5, pore volume distributions were calculated using the DLJ method for the desorption segment of the hysteresis curves in Fig. 5. Results are plotted in Fig. 6. All samples showed homogeneous pore size distributions with maxima in the range of 30–40 nm. This range denotes the presence of mesoporosity in the agglomerates of the prepared nanoparticles [54]. The mono dispersity in the pore size distribution within the agglomerates relatively reflects the homogeneity of the particle size distribution in these samples. No pronounced difference in the pore size or its distribution was observed among samples prepared from solutions containing various concentrations. The homogenous distribution of mesopores in the aggregates of the prepared nanoparticles offers an advantage for these nanoparticles if they are used for environmental applications.

Fig. 7 shows SEM and TEM micrographs of nanoparticles formed in solutions containing 0.075 M/0.15 M and 0.3 M/0.6 M of Fe^{2+}/Fe^{3+}, respectively. The micrographs in Fig. 7a and c show the morphology of the agglomerated nanoparticles whose size increases with increasing the concentration of the

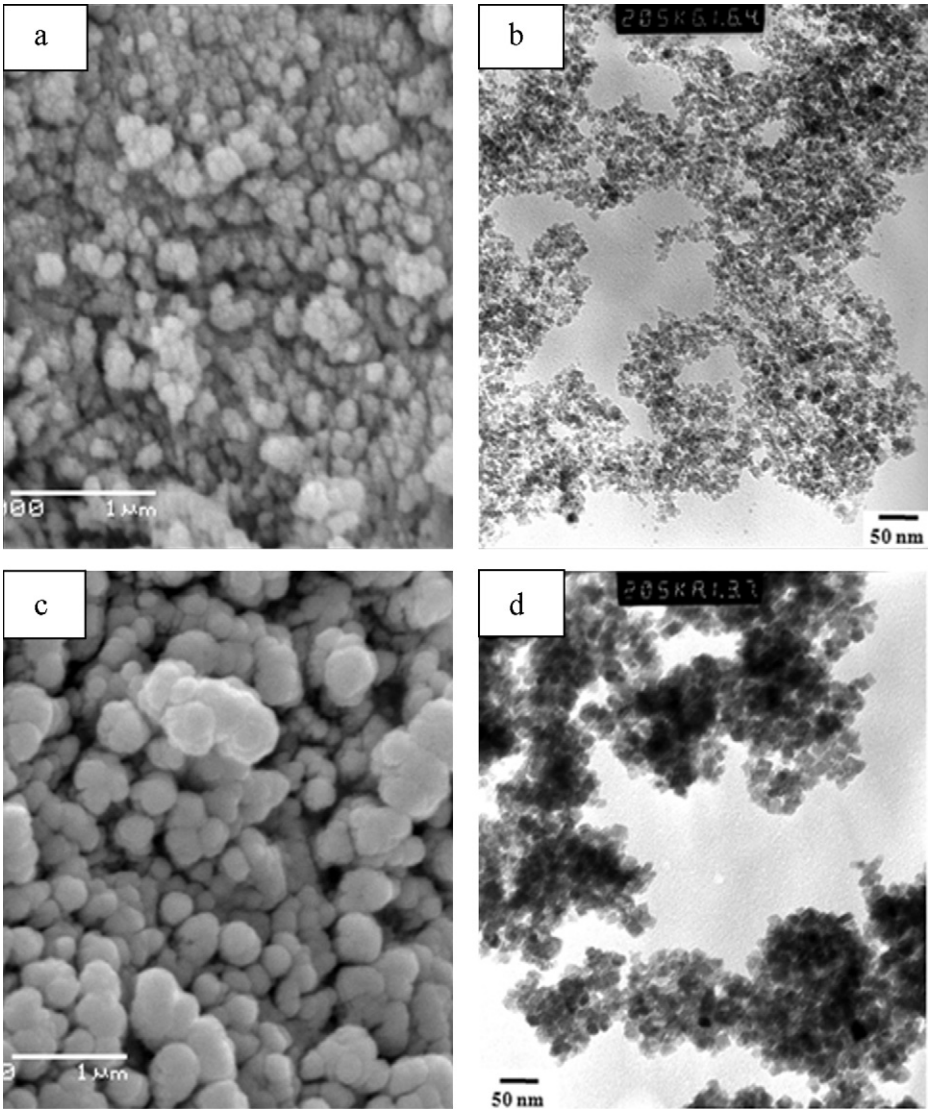

Fig. 7. (a) SEM and (b) TEM micrographs of a magnetite nanoparticles prepared from solutions containing 0.075 and 0.15 mol/L of Fe^{2+} and Fe^{3+}, respectively. (c) SEM and (d) TEM micrographs of magnetite nanoparticles prepared from solutions containing 0.3 and 0.6 mol/L of Fe^{2+} and Fe^{3+}, respectively.

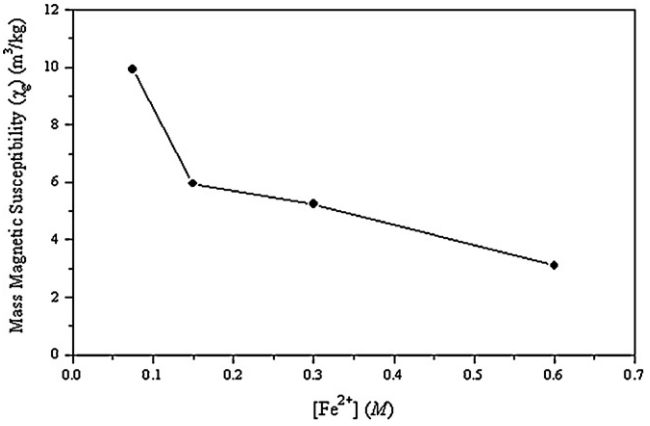

Fig. 8. Magnetic susceptibility of magnetite nanoparticles prepared in solutions containing different initial concentrations of Fe^{2+} and Fe^{3+} ions.

starting reagents. The lowest average size of the agglomerates obtained was of 55 nm as shown in the SEM micrograph in Fig. 7a. Unlike the massive agglomeration observed in the magnetite formed by co-precipitation, ensembles of a maximum of 10 nanoparticles were observed. Agglomeration is explained in terms of the mutual hydrophobic and magnetic interactions between the nanoparticles [52]. Details of these agglomerates are shown in the corresponding TEM micrographs of these samples in Fig. 7b and d. Magnetite nanoparticles shown in Fig. 7 are spherical in shape with a homogeneous size distribution. The average sizes of these nanoparticles were 10 ± 5 and 25 ± 5 nm, for samples prepared from relatively dilute solutions ($Fe^{2+}/Fe^{3+} = 0.075/0.15$) and relatively more concentrated solutions ($Fe^{2+}/Fe^{3+} = 0.3/0.6$), respectively. The relatively smaller particle size shown in Fig. 7b explains the relatively small crystallite size of this sample that was previously shown in Fig. 3.

The magnetic susceptibility results of magnetite samples prepared at different starting concentrations of Fe^{2+} and Fe^{3+} ions are shown in Fig. 8. Magnetic susceptibility is the degree to which a material can be magnetized in an external magnetic field, and is directly proportional to its magnetization [55]. Moreover, the magnetic size is known to be directly proportional to the magnetic susceptibility of solid nanoparticles [56]. Susceptibility data shown in Fig. 8 indicates an opposite behavior, but is still explained by their agglomeration and size characteristics. Previous results by Thapa et al. [57] attributed the increase in the magnetization of magnetite with the decrease of particle size to the decrease in the oxygen content in the magnetite samples and the subsequent increase of $[Fe^{2+}]$ in the magnetite lattice, which is the main cause of magnetic character of magnetite nanoparticles. Moreover, Ma and Liu [58] related the decrease in magnetic properties with increasing size of magnetite nanoparticles to the agglomeration of the particles, which is caused by the hydrophobic interaction between them. The magnetization properties of the currently prepared mesoporous magnetite nanoparticles prepared at the optimized conditions suggest them as potential candidates for both biomedical and environmental applications.

4. Summary

Slightly modified co-precipitation method was used for the preparation of mesoporous magnetite nanoparticles. Precipitation of magnetite took place in air at relatively low temperatures. Despite this fact, no evidence was found for the oxidation of magnetite during or after precipitation. Monolithic magnetite was confirmed by XRD. Results indicated that using a slow feeding rate, for the Fe^{2+}/Fe^{3+} reactants, maintaining the stirring and soaking temperatures at 60 °C, and using initial dilute solutions of the iron species resulted in the formation of nanoparticles with an average agglomerate size of 55 nm and a surface area of 210 m^2/g. This was reflected in a unimodal pore size distribution with an average pore diameter of 38 nm. Detailed TEM results showed that monodisperse nanoparticles of as low as 10 ± 5 nm could be achieved in relatively dilute solutions of the starting Fe^{2+} and Fe^{3+} salts. Magnetic susceptibility measurements at room temperature indicated the magnetization capability of the nanoparticles and its dependence on the size of the particles.

References

[1] S. Sun, C.B. Murray, D. Weller, L. Folks, A. Moser, Monodisperse FePt nanoparticles and ferromagnetic FePt nanocrystal superlattices, Science 287 (2000) 1989–1992.
[2] M.M. Miller, G.A. Prinz, S.F. Cheng, S. Bounnak, Detection of a micron-sized magnetic sphere using a ring-shaped anisotropic magnetoresistance-based sensor: a model for a magnetoresistance-based biosensor, Appl. Phys. Lett. 81 (2002) 2211–2213.
[3] T.K. Jain, M.A. Morales, S.K. Sahoo, D.L. Leslie-Pelecky, V. Labhasetwar, Iron oxide nanoparticles for sustained delivery of anticancer agents, Mol. Pharm. 2 (2005) 194–205.
[4] I. Chourpa, L. Douziech-Eyrolles, L. Ngaboni-Okassa, J.F. Fouquenet, S. Cohen-Jonathan, M. Souce, H. Marchais, P. Dubois, Molecular composition of iron oxide nanoparticles, precursors for magnetic drug targeting, as characterized by confocal Raman microspectroscopy, Analyst 130 (2005) 1395–1403.
[5] J.W. Bulte, Intracellular endosomal magnetic labeling of cells, Methods Mol. Med. 124 (2006) 419–439.
[6] M. Modo, J.W. Bulte, Cellular MR imaging, Mol. Imaging 4 (2005) 143–164.
[7] C. Burtea, S. Laurent, A. Roch, L. Vander Elst, R.N. Muller, C-MALISA (cellular magnetic-linked immunosorbent assay), a new aapplication of cellular ELISA for MRI, J. Inorg. Biochem. 99 (2005) 1135–1144.
[8] S. Boutry, S. Brunin, I. Mahieu, S. Laurent, L. Vander Elst, R.N. Muller, Magnetic labeling of non-phagocytic adherent cells with iron oxide nanoparticles: a comprehensive study, Contrast Media Mol. Imaging 3 (2008) 223–232.
[9] L. Babes, B. Denizot, G. Tanguy, J.J. Le Jeune, P. Jallet, Synthesis of iron oxide nanoparticles used as MRI contrast agents: a parametric study, J. Colloid Interface Sci. 2 (1999) 474–482.
[10] S.W. Charles, J. Popplewell, Properties and applications of magnetic liquids, Endeavour 6 (1982) 153–161.
[11] S. Lim, E. Woo, H. Lee, C. Lee, Synthesis of magnetite-mesoporous silica composites as adsorbents for desulfurization from natural gas, Appl. Catal. B: Environ. 85 (2008) 71–76.
[12] I. Slowing, J. Vivero-Escoto, C. Wu, V. Lin, Mesoporous silica nanoparticles as controlled release drug delivery and gene transfection carriers, Adv. Drug Deliv. Rev. 60 (2008) 1278–1288.
[13] S. Guo, D. Li, L. Zhang, J. Li, E. Wang, Monodisperse mesoporous superparamagnetic single-crystal magnetite nanoparticles for drug delivery, Biomaterials 30 (2009) 1881–1889.
[14] M. Chastellain, A. Petri, A. Gupta, K.V. Rao, H. Hofmann, Superparamagnetic Silica-iron oxide nanocomposites for application in hyperthermia, Adv. Eng. Mater. 6 (2004) 235–241.

[15] J.T. Mayo, C. Yavuz, S. Yean, L. Cong, H. Shipley, W. Yu, J. Falkner, A. Kan, M. Tomson, V. Colvin, The effect of nanocrystalline magnetite size on arsenic removal, Sci. Technol. Adv. Mater. 8 (2007) 71–75.
[16] R. Chen, C. Zhi, H. Yang, Y. Bando, Z. Zhang, N. Sugiur, D. Golberg, Arsenic (V) adsorption on Fe_3O_4 nanoparticle-coated boron nitride nanotubes, J. Colloid Interface Sci. 359 (2011) 261–268.
[17] A.B. Chin, I.I. Yaacob, Synthesis and characterization of magnetic iron oxide nanoparticles via w/o microemulsion and Massart's procedure, J. Mater. Process. Technol. 191 (2007) 235–237.
[18] C. Albornoz, S.E. Jacobo, Preparation of a biocompatible magnetoc film from an aqueous ferrofluid, J. Magn. Magn. Mater. 305 (2006) 12–15.
[19] E.H. Kim, H.S. Lee, B.K. Kwak, B.K. Kim, Synthesis of ferrofluid with magnetic nanoparticles by sonochemical method for MRI contrast agent, J. Magn. Magn. Mater. 289 (2005) 328–330.
[20] J. Wan, X. Chen, Z. Wang, X. Yang, Y. Qian, A soft-template-assisted hydrothermal approach to single-crystal Fe_3O_4 nanorods, J. Cryst. Growth 276 (2005) 571–576.
[21] M. Kimata, D. Nakagawa, M. Hasegawa, Preparation of monodisperse magnetic particles by hydrolysis of iron alkoxide, Powder Technol. 132 (2003) 112–118.
[22] G.S. Alvarez, M. Muhammed, A.A. Zagorodni, Novel flow injection synthesis of iron oxide nanoparticles with narrow size distribution, Chem. Eng. Sci. 61 (2006) 4625–4633.
[23] S. Basak, D.-R. Chen, P. Biswas, Electrospray of ionic precursor solutions to synthesize iron oxide nanoparticles: modified scaling law, Chem. Eng. Sci. 62 (2007) 1263–1268.
[24] A.K. Gupta, S. Wells, Surface-modified superparamagnetic nanoparticles for drug delivery: preparation, characterization, and cytotoxicity studies, IEEE Trans. Nanobiosci. 3 (2004) 66.
[25] S.W. Charles, Magnetic fluids (ferrofluids), in: J.L. Dormann, D. Fiorani (Eds.), Magnetic Properties of Fine Particles, Elsevier, North-Holland, 1992, pp. 267–374.
[26] A.K. Gupta, A.S.G. Curtis, Lactoferrin and ceruloplasmin derivatized superparamagnetic iron oxide nanoparticles for targeting cell surface receptors, Biomaterials 25 (2004) 3029–3040.
[27] K. Nishio, M. Ikeda, N. Gokon, S. Tsubouchi, H. Narimatsu, Y. Mochizuki, S. Sakamoto, A. Sandhu, M. Abe, H. Handa, Preparation of size-controlled (30–100 nm) magnetite nanoparticles for biomedical applications, J. Magn. Magn. Mater. 310 (2007) 2408–2410.
[28] T.K. Jain, M.A. Morales, S.K. Sahoo, D.L. Leslie, V. Labhasetwar, Iron oxide nanoparticles for sustained delivery of anticancer agents, Mol. Pharm. 2 (2005) 194–205.
[29] A.P.A. Faiyas, E.M. Vinod, J. Joseph, R. Ganesan, R.K. Pandey, Dependence of pH and surfactant effect in the synthesis of magnetite (Fe_3O_4) nanoparticles and its properties, J. Magn. Magn. Mater. 322 (2010) 400–404.
[30] Z.T. Tsai, J.F. Wang, H.Y. Kuo, C.R. Shen, J.J. Wang, T.C. Yen, In situ preparation of high relaxivity iron oxide nanoparticles by coating with chitosan: a potential MRI contrast agent useful for cell tracking, J. Magn. Magn. Mater. 322 (2010) 208–213.
[31] J.-P. Jolivet, E. Tronc, C. Chaneac, Synthesis of iron oxide-based magnetic nanomaterials and composites, J. C. R. Chimie 5 (2002) 659–664.
[32] A.K. Gupta, M. Gupta, Synthesis and surface engineering of iron oxide nanoparticles for biomedical applications, J. Biomater. 26 (2005) 3995–4021.
[33] U. Schwertmann, R.M. Cornell, Iron Oxides in the Laboratory: Preparation and Characterization, Wiley, 2000.
[34] F.A. Cotton, G. Wilkinson, Advanced Inorganic Chemistry, Wiley Interscience, New York, 1988.
[35] D.K. Kim, Y. Zhang, W. Voit, K.V. Rao, M. Muhammed, Synthesis and characterization of surfactant-coated superparamagnetic monodispersed iron oxide nanoparticles, J. Magn. Magn. Mater. 225 (2001) 30–36.
[36] M. Pourbaix, Atlas of Electrochemical Equilibria in Aqueous Solutions, NACE International, USA, 1974.
[37] E. Illés, E. Tombácz, The role of variable surface charge and surface complexation in the adsorption of humic acid on magnetite, J. Colloids Surf. A 230 (2003) 99–109.
[38] E. Tombácz, A. Majzik, Z.S. Horvát, E. Illés, Magnetite in aqueous medium: coating its surface and surface coated with it, Rom. Rep. Phys. 58 (2006) 281–286.
[39] E. Tombácz, Adsorption from electrolyte solutions, in: J. Tóth (Ed.), Adsorption: Theory, Modeling, and Analysis, Marcel Dekker, New York, 2002, p. 711.
[40] R.J. Hunter, Foundations of Colloid Science, vol. 1, Clarendon Press, Oxford, 1987.
[41] S. Laurent, D. Forge, M. Port, A. Roch, C. Robic, L. Vander Elst, R.N. Muller, Magnetic iron oxide nanoparticles: synthesis, stabilization, vectorization, physicochemical characterizations, and biological applications, J. Chem. Rev. 108 (2008) 2064–2110.
[42] R.M. Cornell, U. Schertmann, The Iron Oxides: Structure, Properties, Reactions, Occurrences, and Uses, Wiley-VCH, 2003.
[43] R. Boistelle, J.P. Astier, Crystallization mechanisms in solution, J. Cryst. Growth 90 (1988) 14–30.
[44] T. Sugimoto, Formation of monodispersed nano- and micro-particles controlled in size, shape, and internal structure, J. Chem. Eng. Technol. 26 (2003) 313–321.
[45] H.-C. Schwarzer, W. Peukert, Combined experimental/numerical study on the precipitation of nanoparticles, AIChE J. 191 (2004) 3234–3247.
[46] R.M. Cornell, U. Schertmann, Iron Oxides in the Laboratory: Preparation and Characterization, VCH Publishers, Weinheim, Germany, 1991.
[47] N.M. Gribanow, E.E. Bibik, O.V. Buzunov, V.N. Naumov, Physicochemical regularities of obtaining highly dispersed magnetite by the methid of chemical condensation, J. Magn. Magn. Mater. 85 (1990) 7–10.
[48] X.L. Zhang, H.Y. Niu, S.X. Zhang, Y.Q. Cai, Preparation of a chitosan-coated C18-functionalized magnetite nanoparticle sorbent for extraction of phthalate ester compounds from environmental water samples, J. Anal. Bioanal. Chem. 397 (2010) 791–798.
[49] J. Lee, T. Isobe, M. Senna, Preparation of ultrafine Fe_3O_4 particles by precipitation in the presence of PVA at high pH, J. Colloid Interface Sci. 177 (1996) 490–494.
[50] S. Liu, X. Wei, M. Chu, J. Peng, Y. Xu, Synthesis and characterization of iron oxide/polymer composite nanoparticles with pendent functional groups, J. Colloids Surf. B: Biointerfaces 51 (2006) 101–106.
[51] Z.H. Zhou, J. Wang, X. Liu, H.S.O. Chan, Synthesis of Fe_3O_4 nanoparticles from emulsions, J. Mater. Chem. 11 (2001) 1704–1709.
[52] R. Valenzuela, M.C. Fuentes, C. Parra, J. Baeza, N. Duran, S.K. Sharma, M. Knobel, J. Freer, Influence of stirring velocity on the synthesis of magnetite nanoparticles (Fe_3O_4) by the co-precipitation method, J. Alloys Compd. 488 (2009) 227–231.
[53] I. Nedkov, T. Merodiiska, L. Slavov, R.E. Vandenberghe, Y. Kusano, J. Takada, Surface oxidation, size and shape of nano-sized magnetite obtained by coprecipitation, J. Magn. Magn. Mater. 300 (2006) 358–367.
[54] F. Rouquerol, K. Sing, Adsorption by Powders and Porous Solids: Principles, Methodology and Applications, Academic Press, UK, 1999.
[55] P. Blum, Magnetic susceptibility, in: Physical Properties Handbook, 1997 (Chapter 4).
[56] S. Si, A. Kotal, T.K. Mandal, S. Giri, H. Nakamura, T. Kohara, Size-controlled synthesis of magnetite nanoparticles in the presence of polyelectrolytes, J. Chem. Mater. 16 (2004) 3489–3496.
[57] D. Thapa, V.R. Palkar, M.B. Kurup, S.K. Malik, Properties of magnetite nanoparticles synthesized through a novel chemical route, J. Mater. Lett. 58 (2004) 2692–2694.
[58] Z. Ma, H. Liu, Synthesis and surface modification of magnetic particles for application in biotechnology and biomedicine, J. China Particuol. 5 (2007) 1–10.